Title	Optimization Assessment Memo		
Document No.	DE-EE0006610 M5.5 Optimization Memo		
Version	1.1		
Prime Contract	DE-EE0006610		
Authored	Pukha Lenee-Bluhm		
Reviewed	E. Hammagren, K. O'Hearn, B. Lamb, M. Ondusko		
Version Approved			
Data Classification	☐ Limited Rights Data	☒ Protected Data	☐ Public Data

Version	Date	Summary
1.0	10/31/2019	Release with Final Reporting

TABLE OF CONTENTS

TABLE OF FIGURES

TABLE OF TABLES

1 INTRODUCTION

Columbia Power Technologies, Inc. (C·Power) is developing a direct drive, rotary wave energy converter (DDR-WEC) for utility-scale power applications, known as the StingRAY. The DE-EE0006610 Project objectives are to improve the overall Power-to-Weight (PWR) ratio and decrease Levelized Cost of Energy (LCOE). This will be achieved by decreasing capital expenditures (CAPEX), reducing structural mass, and increasing performance.

A hybrid structure was conceptualized as a means of cost and weight reduction, in which fiber reinforced plastic (FRP) replaces steel in sections of cylindrical hull components between complex joints with high strength and stiffness requirements, and a supportive program of structural testing undertaken.

The objective of this document is to present the design validation and optimization enabled by Project structural testing. Please note that the test report is a separate document in which the test methodology and results are detailed; the present document covers work utilizing the test results to enable engineering analysis. The structural testing was composed of two phases: coupon testing, and full-scale sectioned joint testing.

Extensive coupon testing was performed to validate material properties of the constituent plies proposed for the fiber-reinforced plastic (FRP) laminate. The measured material properties were then used to optimize the laminate layup for the hybrid pontoon design developed previously. The establishment of design values from coupon test results, and subsequent laminate optimization, are discussed in section 2.

Full-scale sectioned joint specimens were tested to verify the feasibility of the double lap shear joint design and to compare the performance of the candidate adhesives. Adhesive joint testing, and design feasibility, are discussed in section 3.

The potential impact of the structural testing and optimization on the StingRAY H2 WEC is discussed in section 4. The hybrid structure concept is extended to similar components and impacts on weight and cost are assessed.

2 LAMINATE MATERIAL PROPERTIES AND OPTIMIZATION

2.1 Introduction

The hybrid pontoon concept design was based on Project structural design loads, using constituent materials and fabrication procedures as specified by an FRP partner (Ershigs); the concept design is documented in *Test Article Design* [1]. The pontoons are cylindrical, and the concept laminate is composed of layers of two different constituent materials. The first is E-glass (CPIC ER 469LV-2000) wound at ± 65° from the mandrel axis with an epoxy vinyl ester resin (Ashland Derakane 411). The second is a stitched unidirectional E-glass fabric (Vectorply E-T 1600) hand laid on the mandrel with fibers parallel to the mandrel axis. A stitched quadraxial E-glass fabric (Vectorply E-QX 10200) may be utilized in the future for fabricated internal stiffening details, though it is not included in the current design.

For the concept design, constituent ply material properties were estimated using manufacturers' specification sheets, in accordance with guidelines published in *DNVGL-ST-C501 Composite Components* (C501) [2]. The concept layup schedule was specified as [1FW,9(1U,2FW)], where FW indicates a full layer of filament-wound E-glass and U a layer of the unidirectional Vectorply fabric.

Composite laminate properties are heavily dependent on the constituent materials and the processes used to combine them. Structural testing was undertaken to allow for an optimization of the laminate based on laboratory observations of material properties. Testing was performed on filament wound (FW),

uniaxial (UNI), and quadraxial (QUAD) coupons. The QUAD coupon results are not covered in this document, as they were not utilized in the concept design or subsequent optimization. Coupon specifications (layup and dimensions) are detailed in *WEC Pontoon Design Alternative Composites Coupon Panels* [3]. Testing procedures and detailed results, including photos and descriptions of failure modes, are covered in *C·Power Coupon and Double Lap Shear Specimen Test Report* [4].

2.2 Characteristic Values of Material Properties

The structural analysis described in this document is based upon characteristic values of material properties derived from the laboratory test results, following guidance from C501. For elastic properties, the characteristic values are simply the mean value of valid test results (C501 4.2.4.6). For strength properties, the characteristic value is reduced from the mean by a specified number (k_m) of standard deviations (C501 4.2.4.5). Specific values of k_m depend upon the number of valid test results and are taken from C501 Table 4-3. Alternate k_m values are taken from C501 Table 4-5 for tensile strength in the fiber direction, as allowed by C501 4.2.7. Relevant test results, along with the characteristic values, are detailed in Table 1 and Table 2 below; in these tables 'direction 1' refers to the fiber warp (for FW this is 65° off mandrel axis, for UNI this is parallel to the mandrel axis) and 'direction 2' is in-plane and orthogonal. Details on the data used to determine the characteristic values can be found in the *Test Report* [4]. Note that FW tensile strength perpendicular to the fibers (direction 2) was not tested but assumed to be similar to UNI as this is a matrix dominated property and the same resin was used for both.

Table 1 – Material properties determined from filament wound (FW) coupons.

Property	Units	Mean	std	pstd	N tests	k_m	Char. value	Test Report [4] source
Elastic modulus, dir. 1 (E_1)	GPa	26.0	1.38	0.05	5	-	26.0	D3039, Table 2-5
Elastic modulus, dir. 2 (E_2)	GPa	16.8	2.34	0.14	5	-	16.8	D6641, Table 3-3
Shear modulus, 1-2 plane (G_{12})	GPa	5.93	0.59	0.10	8	-	5.93	D7078, Table 4-6
Poisson's ratio, 1-2 plane (ν_{12})	-	0.503	0.055	0.11	4	-	0.503	D3039, Table 2-5
Tensile strength, dir. 1 ($\hat{\sigma}_{1t}$)	MPa	503	22.7	0.05	5	2.3	451	D3039, Table 2-3
Compressive strength, dir. 1 ($\hat{\sigma}_{1c}$)	MPa	371	50.2	0.14	8	2.6	241	D6641, Table 3-3
Tensile strength, dir. 2 ($\hat{\sigma}_{2t}$)	MPa	20.6	2.03	0.10	6	2.8	14.9	UNI result, see below
Compressive strength, dir. 2 ($\hat{\sigma}_{2c}$)	MPa	113	17.7	0.16	8	2.6	66.6	D6641, Table 3-3
Shear strength, 1-2 plane ($\hat{\sigma}_{12}$)	MPa	108	11.4	0.11	8	2.6	78.0	D7078, Table 4-6

Table 2 – Material properties determined from uniaxial (UNI) coupons.

Property	Units	Mean	std	pstd	N tests	k_m	Char. value	Test Report [4] source
Elastic modulus, dir. 1 (E_1)	GPa	32.8	4.69	0.14	8	-	32.8	D3039, Table 2-5
Elastic modulus, dir. 2 (E_2)	GPa	8.20	1.03	0.13	4	-	8.20	D6641, Table 3-3
Shear modulus, 1-2 plane (G_{12})	GPa	2.00	0.05	0.03	8	-	2.00	D7078, Table 4-7
Poisson's ratio, 1-2 plane (ν_{12})	-	0.418	0.020	0.05	8	-	0.418	D3039, Table 2-5
Tensile strength, dir. 1 ($\hat{\sigma}_{1t}$)	MPa	573	26.2	0.05	8	2.2	515	D3039, Table 2-3
Compressive strength, dir. 1 ($\hat{\sigma}_{1c}$)	MPa	306	25.7	0.08	7	2.8	234	D6641, Table 3-3
Tensile strength, dir. 2 ($\hat{\sigma}_{2t}$)	MPa	20.6	2.03	0.10	6	2.8	14.9	D3039, Table 2-11
Compressive strength, dir. 2 ($\hat{\sigma}_{2c}$)	MPa	75.9	3.36	0.04	8	2.6	67.2	D6641, Table 3-3
Shear strength, 1-2 plane ($\hat{\sigma}_{12}$)	MPa	35.8	1.57	0.04	8	2.6	31.7	D7078, Table 4-7

In addition to the elastic and strength material properties, the measured thickness and density of the constituent materials are relevant to the laminate design and optimization. Measured thickness, density, and fiber volume fraction (FVF) are listed in Table 3. Thickness values presented are the mean of all tensile, compression, and shear coupons (32 coupons for each material, see the *Test Report* [4] for details), and are normalized to represent one complete layer for each material. Density and FVF measurements and calculations are described in section 9 of the *Test Report* [4].

Table 3 – Thickness, density, and FVF for FW and UNI materials.

	Thickness [mm]	Density [kg/m^3]	FVF
FW	1.44	1880	0.509
UNI	0.797	1540	0.291

2.3 Finite Element Analysis Setup

2.3.1 Overview

The Finite Element Analysis (FEA) discussed in this document was carried out following guidance from C501. The analysis was generally similar to that performed by Glosten for the hybrid pontoon concept design [1] but differed in several ways which will be covered in relevant sections. The two most significant differences, aside from the use of characteristic values derived from test results, are briefly highlighted here:

- The load and resistance partial safety factors in the present analysis follow more closely to those utilized in the prototype steel design, and are significantly larger than those used for the hybrid pontoon concept design, and
- The load cases in the present analysis follow more closely to those utilized in the prototype steel design; the load cases used for hybrid pontoon concept design grossly exaggerated structural loading.

ANSYS Mechanical v16 was used to mesh, analyze, and post-process the results.

2.3.2 Failure Criterion

The Tsai-Wu failure criterion (TWFC) was used to evaluate laminate failure in lieu of maximum strain requirements, following guidance in C501 6.3.3. The equations used to evaluate 2D TWFC are given in Figure 1.

The safety factor, R, is calculated as the product of several partial safety factors. The partial load effect factor, γ_F, is given a different value for different load cases (which are discussed in 2.3.5); the partial load effect factors are taken from the prototype steel WEC design analysis (*WEC Design Documentation* [5]). For general loading (derived from the 50-year storm design case) $\gamma_F = 1.35$, for slamming pressure $\gamma_F = 1.5$, and for hydrostatic pressure $\gamma_F = 1.2$. The partial resistance factor $\gamma_M = 1.22$, per C501 Table 8-6. The load model factor $\gamma_{Sd} = 1$ for FEA, per C501 9.12.3.2. The parameter H^*_{12} was assigned a default value of -0.5 and thus the resistance model factor $\gamma_{Rd} = 1.15$, per C501 6.3.3.4.

The safety factor, R, is thus equal to 1.89, 2.10, or 1.65 depending on the load case. Note that the concept design used a combined partial load and resistance safety factor (product of γ_F and γ_M) of 1.11, resulting in a significantly lower R = 1.28 (used for all load cases).

$$R^2\left(F_{11}\sigma_1^2 + F_{22}\sigma_2^2 + F_{12}\sigma_{12}^2 + 2H_{12}\sigma_1\sigma_2\right) + R\left(F_1\sigma_1 + F_2\sigma_2\right) < 1$$

$$R = \gamma_F \cdot \gamma_{Sd} \cdot \gamma_m \cdot \gamma_{Rd}$$

$$F_{11} = \frac{1}{\hat{\sigma}_{1t}\,\hat{\sigma}_{1c}}, \quad F_{22} = \frac{1}{\hat{\sigma}_{2t}\,\hat{\sigma}_{2c}}, \quad F_{12} = \frac{1}{\hat{\sigma}_{12}^2}$$

$$H_{12}^* = \frac{H_{12}}{\sqrt{F_{11}F_{22}}}, \quad F_1 = \frac{1}{\hat{\sigma}_{1t}} - \frac{1}{\hat{\sigma}_{1c}}, \quad F_2 = \frac{1}{\hat{\sigma}_{2t}} - \frac{1}{\hat{\sigma}_{2c}}$$

where:

n	ply co-ordinate system direction
σ_n	characteristic value of the local load effect of the structure (stress) in the direction n
$\hat{\sigma}_{nt}$	characteristic tensile strength in the direction n
$\hat{\sigma}_{nc}$	characteristic compressive strength in the direction n
$\hat{\sigma}_{nk}$	characteristic shear strength in the direction nk
γ_F	partial load effect factor
$\gamma_{Sd,}$	partial load-model factor
γ_M	partial resistance factor
γ_{Rd}	partial resistance-model factor

Figure 1 – Tsai Wu Failure Criterion (DNVGL-ST-C501).

The characteristic material properties from Table 1 and Table 2 were used in calculating TWFC, with two modifications. First, characteristic strength in the fiber direction ($\hat{\sigma}_{1t}$ and $\hat{\sigma}_{1c}$) was reduced by 10% to account for long term water saturation, per C501 4.5.3. Second, modified values were used for in-plane strength perpendicular to the fiber warp ($\hat{\sigma}_{2t}$ and $\hat{\sigma}_{2c}$), per C501 6.3.3.5 (see Figure 2), using moduli of elasticity (E_1 and E_2).

$$\hat{\sigma}_{2t} = \frac{E_2}{E_1}\hat{\sigma}_{1t} \qquad \hat{\sigma}_{2c} = \frac{E_2}{E_1}\hat{\sigma}_{1c}$$

Figure 2 – Modified in-plane strength perpendicular to fiber warp (DNVGL ST C501).

2.3.3 Finite Element Analysis Model Setup

FEA model geometry covered the extent of the cylindrical pontoon extending between the interior watertight bulkheads (see sheet 2 of prototype *WEC Structural Arrangement* [6]). The outer diameter is 3.82 m, and the length is 7.90 m. Note that the concept design used slightly smaller dimensions of 3.8 and 7.7 m.

The global coordinate system orientation is indicated in Figure 3 below: the cylinder axis is aligned with x-direction, the z-direction is vertically up from the still-water plane, and the y-direction is orthogonal and in the waterplane. The origin is at the center of the cylinder's axis, and the still water plane is x-y plane at z = 0 (bisecting the cylindrical pontoon section). The element coordinate system is cylindrical, with the x-direction identical to global x-direction, z-direction radial, and y-direction tangential. The solution

coordinate system rotates about the element z-direction such that the solution coordinate x-direction aligns with the fiber warp at each layer.

Shell elements (SHELL181) are used to model the laminate. The elements are quadrilaterals with a nominal dimension of 25 mm square. The mesh is depicted in Figure 3, with detail in Figure 4.

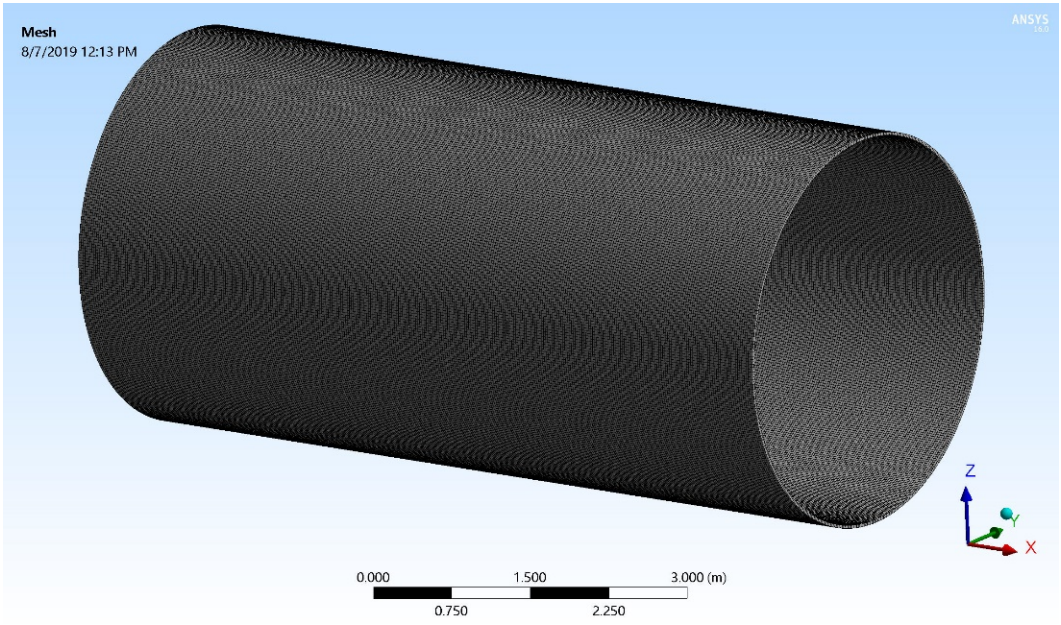

Figure 3 – Global coordinate system, and meshed pontoon model.

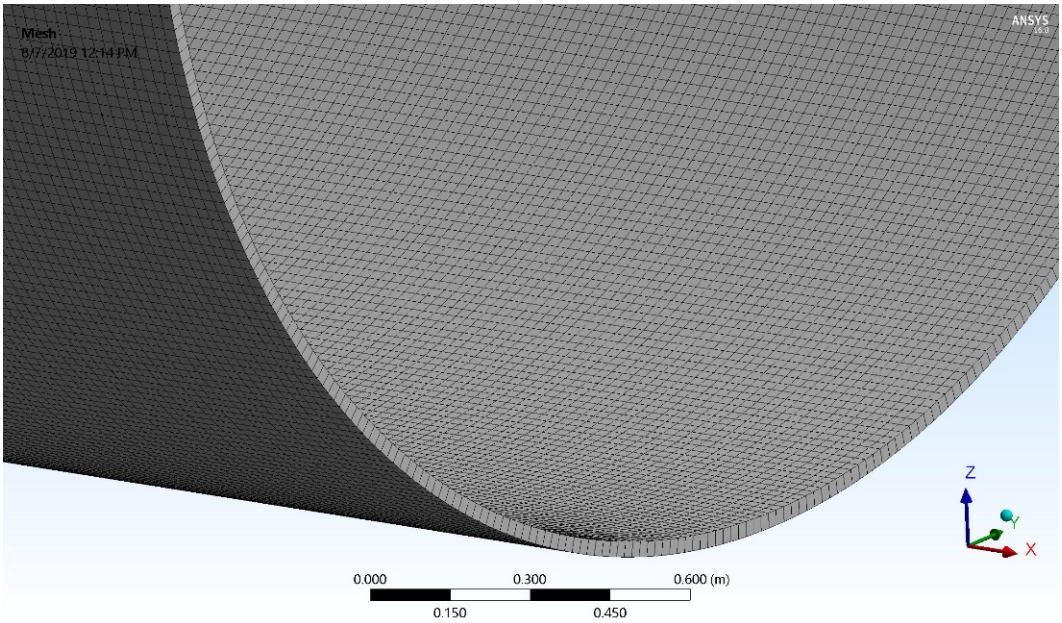

Figure 4 – Detail of 25 mm square, quadrilateral mesh.

The laminate is modeled as layers, corresponding to the constituent plies. Each layer is specified by material type, thickness, and fiber warp direction. The modeled filament wound layers are each one-half

of a complete wound layer and are always used in pairs with ± 65° orientation, in accordance with the fabrication process. The optimized laminate follows the same general layup pattern as the concept laminate, originally specified by our FRP fabrication partner Ershigs: winding begins with a full layer of FW, and then the laminate is built up in sets of a layer of UNI and two full layers of FW. Note that practical fabrication would likely start with laying down a layer of chopped strand mat (CSM) followed by Nexus veil, but that these layers provide no appreciable strength and were not included in the test specimens. Note as well that the optimized laminate has only a single full layer of FW in the last pass [1FW, 7(1U,2FW), 1U, 1FW]. A screenshot detailing the layer setup is given in Figure 5.

Layer	Material	Thickness (m)	Angle (°)
(+Z)			
40	FW_obs	0.0007206	-65
39	FW_obs	0.0007206	65
38	HL_obs	0.0007967	0
37	FW_obs	0.0007206	-65
36	FW_obs	0.0007206	65
35	FW_obs	0.0007206	-65
34	FW_obs	0.0007206	65
33	HL_obs	0.0007967	0
32	FW_obs	0.0007206	-65
31	FW_obs	0.0007206	65
30	FW_obs	0.0007206	-65
29	FW_obs	0.0007206	65
28	HL_obs	0.0007967	0
27	FW_obs	0.0007206	-65
26	FW_obs	0.0007206	65
25	FW_obs	0.0007206	-65
24	FW_obs	0.0007206	65
23	HL_obs	0.0007967	0
22	FW_obs	0.0007206	-65
21	FW_obs	0.0007206	65
20	FW_obs	0.0007206	-65
19	FW_obs	0.0007206	65
18	HL_obs	0.0007967	0
17	FW_obs	0.0007206	-65
16	FW_obs	0.0007206	65
15	FW_obs	0.0007206	-65
14	FW_obs	0.0007206	65
13	HL_obs	0.0007967	0
12	FW_obs	0.0007206	-65
11	FW_obs	0.0007206	65
10	FW_obs	0.0007206	-65
9	FW_obs	0.0007206	65
8	HL_obs	0.0007967	0
7	FW_obs	0.0007206	-65
6	FW_obs	0.0007206	65
5	FW_obs	0.0007206	-65
4	FW_obs	0.0007206	65
3	HL_obs	0.0007967	0
2	FW_obs	0.0007206	65
1	FW_obs	0.0007206	-65
(-Z)			

Figure 5 – Layer specification for optimized laminate in the FEA model.

2.3.4 Boundary Conditions

For all load cases, the pontoon cylinder is fixed at the near end in translation and rotation, approximating the stiffness of the 150 mm steel double flange. The rigid, fixed boundary condition extends 150 mm

axially from the near end. Loading is applied as discussed in the following section (2.3.5) at the far end to achieve the required load conditions at the near end.

For the pressure loading cases, the far end is fixed as well. The fixed far end boundary condition extends over 150 mm, in a manner identical to the near end condition. The pressure loading applied is discussed in the following section (2.3.5).

2.3.5 Design Load Cases

Loads are applied through a rigid interface at the far end, extending 150 mm axially. The rigid interface approximates the double steel flange and assures that the maximum strain will be realized at the near end boundary.

The design load cases (DLCs) used here are taken from the prototype steel WEC design analysis (described in *Design Documentation* [5]). The applied loads and boundary conditions (BC) are given in the upper portion of Table 4, and the reaction loads realized at the near end are given in the lower portion. The first five DLCs are instances from simulations in extreme seas (50-year return period design sea state) that maximize structural loading in each degree of freedom, along with concurrent loading in other degrees of freedom. These DLCs include a corrective moment about the y-axis to ensure the required reaction loads are correct.

Load case six simulates extreme pressure on the bottom of the pontoon during a slamming event. A pressure of 134 kPa is applied uniformly to an arc section of 15°, along the entire length of the pontoon. Load case seven simulates the pontoon under hydrostatic loading from extreme submersion; a pressure of 101 kPa is applied uniformly to the outer surface of the pontoon.

Table 4 – Load cases for hybrid pontoon optimization.

Applied loads

DLC	Description	Fx [kN]	Fy [kN]	Fz [kN]	Mx [kNm]	My [kNm]	Mz [kNm]	Boundary condition	Pressure
1	Max bending	161	0	876	-35.2	968	0	fixed-free	none
2	Max shear	497	0	894	-47.8	-2170	0	fixed-free	none
3	Max axial (tension)	-468	0	619	152	-1200	0	fixed-free	none
4	Max axial (compression)	866	0	426	-63.5	-2790	0	fixed-free	none
5	Max torsion	155	0	372	-299	-2180	0	fixed-free	none
6	Slamming	0	0	0	0	0	0	fixed-fixed	slam
7	Hydrostatic	0	0	0	0	0	0	fixed-fixed	hydro

Reaction loads (at near end)

DLC	Description	Fx [kN]	Fy [kN]	Fz [kN]	Mx [kNm]	My [kNm]	Mz [kNm]
1	Max bending	-161	0	-876	35.2	-7760	0
2	Max shear	-497	0	-894	47.8	-4760	0
3	Max axial (tension)	468	0	-619	-152	-3600	0
4	Max axial (compression)	-866	0	-426	63.5	-518	0
5	Max torsion	-155	0	-372	299	-705	0
6	Slamming	-43.7	0	-236	0	-225	0
7	Hydrostatic	-887	0	0	0	0	0

Note that the DLCs used in the concept design differed significantly from what is presented here. Firstly, for the concept design it was assumed that the maximum shear could occur in the y- or z-direction, but that the specified M_y reaction moment would be maintained in either case. The horizontal maximum shear

cases resulted in artificially excessive moment loads, as the horizontal shear load induced a moment (M_z) in addition to the applied moment (M_y). The load cases in the present analysis reflect an understanding that shear loading on the pontoon is dominated by vertical loading and this is the primary source of moment loading; thus, no horizontal shear cases are included.

Secondly, loading for the concept design was further over-represented by adding hydrostatic pressure loading over the lower half-arc of the pontoon. The design loads are structural reaction loads and already include the effect of hydrostatic pressure, and so the addition of hydrostatic pressure to uncorrected applied loads is unnecessary and overly conservative. Instead, the load cases in the present analysis include the submerged hydrostatic-only case that was used for the prototype steel hull design and do not apply a separate hydrostatic force in the other DLCs.

Finally, the concept design applied the slamming pressure over a 60° arc segment, resulting in an unnecessarily conservative over-loading of the structure. The present analysis applies the slamming pressure over a 15° arc segment (which is the intended DLC and is identical to the prototype steel hull design).

2.4 Results and Discussion

2.4.1 Laminate Optimization

Various laminate layups were modeled and post-processed for TWFC as described above (see 2.3), to determine the fewest layers necessary to keep the maximum TWFC below unity. The resulting optimized laminate [1FW,7(1U,2FW),1U,1FW] utilizes fewer layers overall than the concept design [1FW,9(1U,2FW)].

The maximum TWFC for the optimized laminate is calculated as 0.88 in the most limiting case (slamming pressure). The TWFC distribution for DLC 6 (slamming pressure), for the outermost layer (where the maximum TWFC occurs), is depicted in Figure 6. A summary of the maximum TWFC for all DLCs is presented in Table 5. Note that the maximum TWFC occurs in the outermost UNI layer for most load cases but occurs in the outermost FW layer for the slamming case. TWFC distributions for all DLCs, for the layer with maximum TWFC, are included as Appendix 7.1.

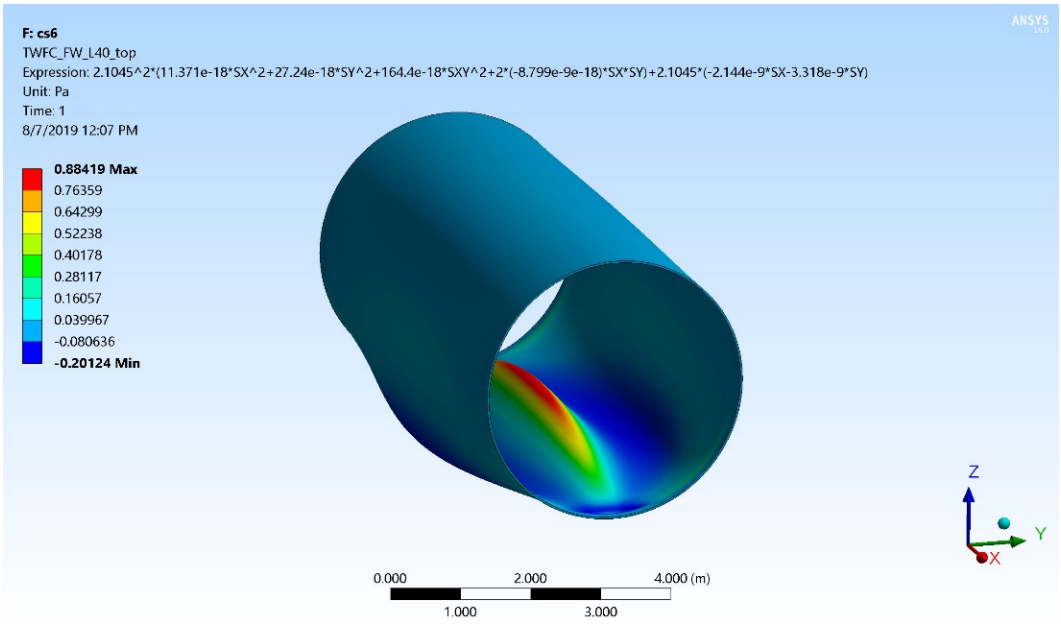

Figure 6 – Tsai Wu Failure Criteria for slamming design load case (DLC 6).

Table 5 – Maximum Tsai Wu Failure Criteria

DLC	Description	R	TWFC
1	Max bending	1.89	0.45
2	Max shear	1.89	0.29
3	Max axial (tension)	1.89	0.17
4	Max axial (compression)	1.89	0.16
5	Max torsion	1.89	0.10
6	Slamming	2.10	0.88
7	Hydrostatic	1.68	0.06

The thickness of the optimized laminate is calculated as 29.4 mm, using the constituent ply thicknesses measured in testing (Table 3). The mass of an FRP pontoon section (7.90 m long by 3.82 m outer diameter) is estimated as 5.04 tonnes based on the constituent layer densities measured in testing (Table 3).

Note that the as-built constituent layers were approximately 30% thicker than specified in design, indicating that they are more resin-rich than anticipated. Per the fabricator, Corrosion Companies Inc (CCI), the reason is likely the large dimensions of the pontoon such that the resin significantly cured before each next layer was wound and thus each next layer rested on top of the old rather than being pulled somewhat into it. Note that in winding the test components, CCI intentionally waited between layers to approximate the fabrication conditions expected for a full pontoon; the smaller size of the as-built test components would have allowed a shorter time between layers, but this would have resulted in a somewhat different product than anticipated for full-scale fabrication. As the laminate strength is fiber dominated, there is potential to develop future process improvements that reduce the resin content and component mass without compromising strength.

2.4.2 Joint Loading

Design loads for the adhesive bond are derived from the FEA described above. Nodal loading along the fixed boundaries, for the limiting design case, is depicted in Figure 7. Note that loading is dominated by shear, justifying the lap shear joint design concept.

Nodal loads at the fixed boundaries are applied to a discretized area representative of the double lap shear joint (DLS), resulting in a bondline stress distribution about the circumference of the bonded joints. The steel flanges from the conceptual design are 150 mm deep and the FEA element size is 25 mm square, resulting in a discretized bond area of 2 * 150 mm * 25 mm = 7500 mm^2. Mean bondline stress in the discretized area of maximum nodal loading is presented in Table 6 for each DLC. DLS test results and design feasibility will be discussed further in section 3.

Table 6 – Maximum bondline stress (from FEA).

DLC	Description	Max. load [kN]	Max. bondline stress [MPa]
1	Max bending	17.1	2.29
2	Max shear	11.3	1.51
3	Max axial (tension)	8.71	1.16
4	Max axial (compression)	2.87	0.383
5	Max torsion	1.93	0.258
6	Slamming	17.6	2.35
7	Hydrostatic	1.89	0.252

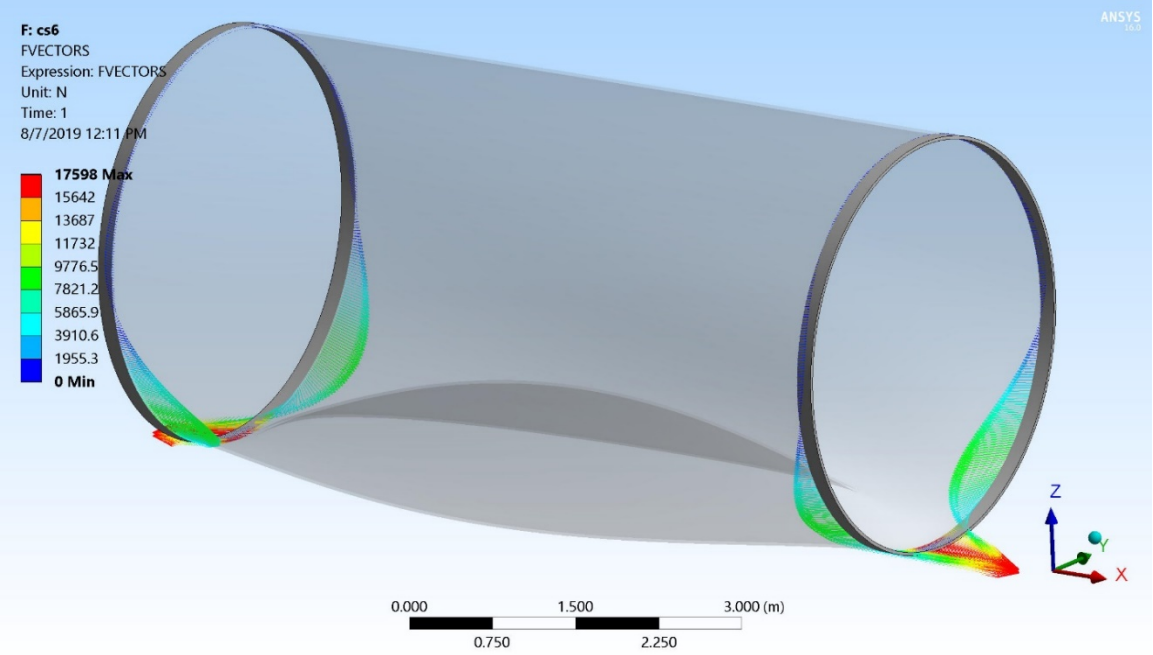

Figure 7 – Force vectors at double lap shear bonded joint.

3 ADHESIVE JOINT FEASIBILITY

3.1 Introduction

The concept joint design is double lap shear (DLS), consisting of two steel rings capturing the edge of the FRP pontoon shell (see Figure 8). The DLS tests are designed to provide full-scale results, with each specimen consisting of a nominally 25.4 mm (1.00 in.) wide section of the full-scale joint. Due to the limitations of the load frame grips and the thickness the FRP, the relative positions (inner and outer) of the steel and FRP were swapped (so that the grips could be used on the steel); a photograph of a DLS specimen installed in the MTS load frame for static testing is shown in Figure 9.

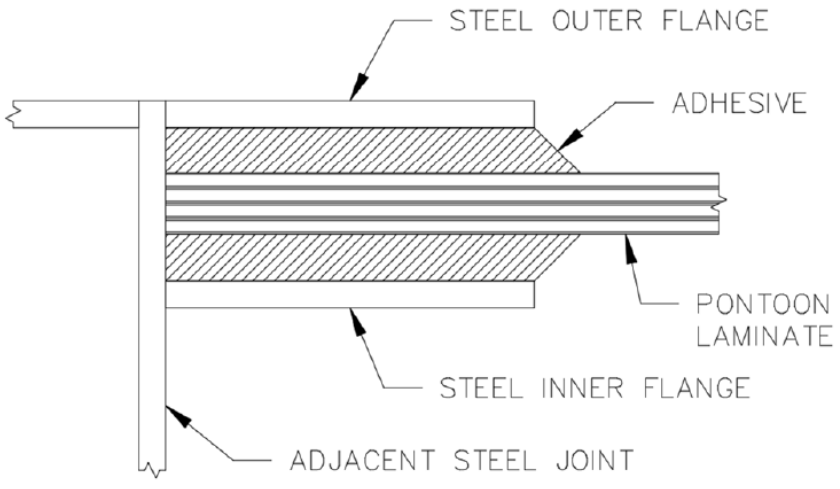

Figure 8 – Double lap shear joint concept detail [1].

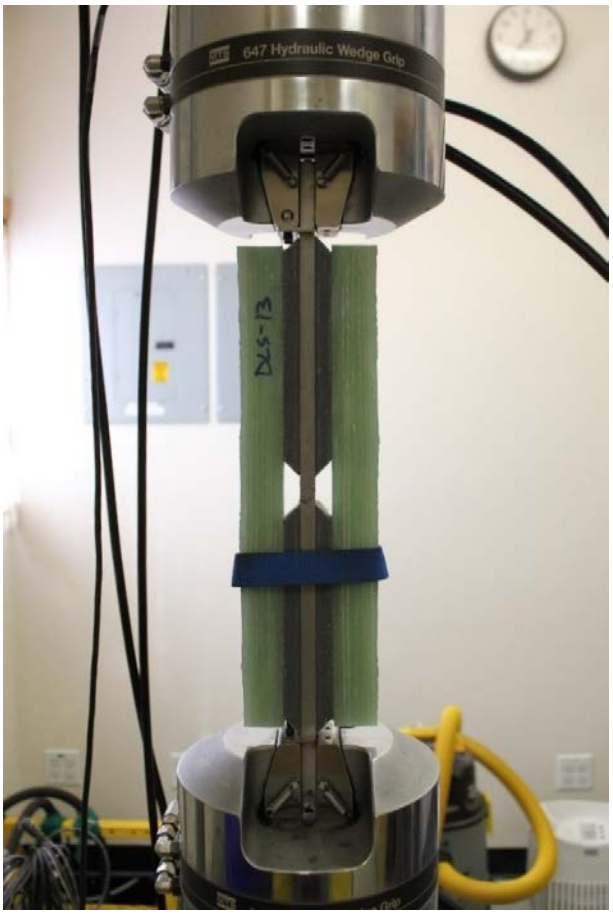

Figure 9 – DLS specimen installed in the MTS load frame for static testing.

Three different adhesives were tested as candidates for the DLS joint designed to facilitate a hybrid steel and FRP pontoon structure. The candidate adhesives were selected on the basis of:

- strength in conjunction with structural adherends (steel and vinyl-ester resin FRP),
- working time,
- gap-filling,
- low-temperature post-cure (room temperature preferred)
- marine applicability,
- shock tolerance (i.e. low modulus).

The large diameter structural components will necessarily deviate from ideal geometry (e.g., diameter, concentricity, eccentricity, etc.), especially the FRP. To accommodate practical fabrication and manufacturing, and avoid unnecessary and costly tolerances, significant gap-filling capability is preferred (allowing for greater bondline thickness). Thus, the intent of the testing was to test over a range of thicknesses and identify adhesives with sufficient strength at significant thicknesses. A range of 6.35 to 19.0 mm (0.250 to 0.750 in.) was selected for testing.

Strengths reported on manufacturers' data sheets were not directly applicable to our design as they are based on testing of very thin bondline thicknesses (on the order of 0.1 to 1 mm) which are not practical for the large diameter structural components under consideration.

Plexus MA560-1 is a two-part methacrylate adhesive designed for bonding thermoplastic, metal, and composite assemblies. It has a working time of 70 minutes (at 23 °C), and is commonly used in FRP boat fabrication with bondline thicknesses up to 1 in. It is relatively flexible, with a specified modulus of 172 to 345 MPa.

Araldite 2013 and 2015 are both two-part epoxy paste adhesives. 2013 is designed for bonding metals, but also suitable for other materials including plastics. 2015 is designed for bonding dissimilar materials generally and is particularly well-suited for FRP. 2013 and 2015 have working times of 80 and 40 minutes, respectively. The Araldite adhesives are described as 'non-sagging' up to 10.0 mm (0.394 in.), and are significantly stiffer than Plexus, with stated shear moduli of 2500 and 900 MPa, respectively.

A bondline length of 152 mm (6.00 in.) was specified in design, and adhesive thicknesses of 6.35, 12.7, and 19.0 mm (0.250, 0.500, and 0.750 in.) were tested. The two Araldite adhesives were only tested at 6.35 and 12.7 mm bondline thickness, on the recommendation from the manufacturer.

3.2 Results and Discussion

3.2.1 Ultimate Limit

The expected stress distribution circumferentially around the adhesive joint is estimated from FEA, and these results are discussed above in 2.4.2. The slamming load case drives the design and results in a characteristic ultimate stress of 2.35 MPa. Note that this is a mean stress calculated over a discretized bond area of 25 (circumferential) by 150 mm (axial).

Adhesive bond theory (specifically, the improved shear-lag based solution for double lap shear joints [7]) was used to estimate the axial stress distribution, utilizing nominal dimensions and published stiffness values. The maximum shear stress, relative to the mean stress, is expected to rise with increasing adhesive stiffness. For a thickness of 12.7 mm (0.500 in.), the ratio of maximum to mean shear stress is calculated as 1.2, 1.6, and 2.1 for Plexus MA560, Araldite 2015, and Araldite 2013 respectively. For a thickness of 6.35 mm (0.25 in.) the maximum stresses increase by about 20%, and for a thickness of 19.0 mm (0.75 in.) the maximum stresses decrease by about 10%. The maximum stress is expected at the inboard end of the bond.

Strain gauges were installed along select DLS bondlines and the data recorded support the theoretical analysis; these data are presented in chapter 7 of the *Test Report* [4]. Typically, the maximum strain was observed at the inboard end and was roughly twice that of the minimum strain observed. However, it is difficult to draw detailed conclusions as the strain was measured at only three locations along select bondlines, and the area covered by a shear strain gauge (5.72 by 8.13 mm) was substantial in comparison to the bondline dimensions. In the present analysis, assessment of DLS strength is based on mean stress over the bonded area.

A total of five DLS specimens were tested for each adhesive configuration (except in the case of 12.7 mm thick Plexus MA560-1 and Araldite 2013, where six specimens were tested). Testing was conducted following guidance from ASTM D5868 and is detailed in chapter 7 of the *Test Report* [4]. To evaluate the shear strength a nominal bond area of 7350 mm^2 (11.4 in^2) is assumed (2 parallel bondlines, 152 mm length by 24.1 mm width). Note that the width was reduced from 25.4 to 24.1 mm (1 in. to 0.95 in.) to ensure a smooth surface and rectangular shape to the steel blanks, as the waterjet cutting produced a slight taper through the thickness (see chapter 6 of the *Test Report* [4] for details of DLS specimen fabrication).

Test specimens were loaded to failure. Typically, the steel-to-adhesive bond was observed to be the primary failure. Descriptions of DLS specimen failures are detailed in the *Test Report* [4], Table 7-4. A typical failure is depicted below in Figure 10.

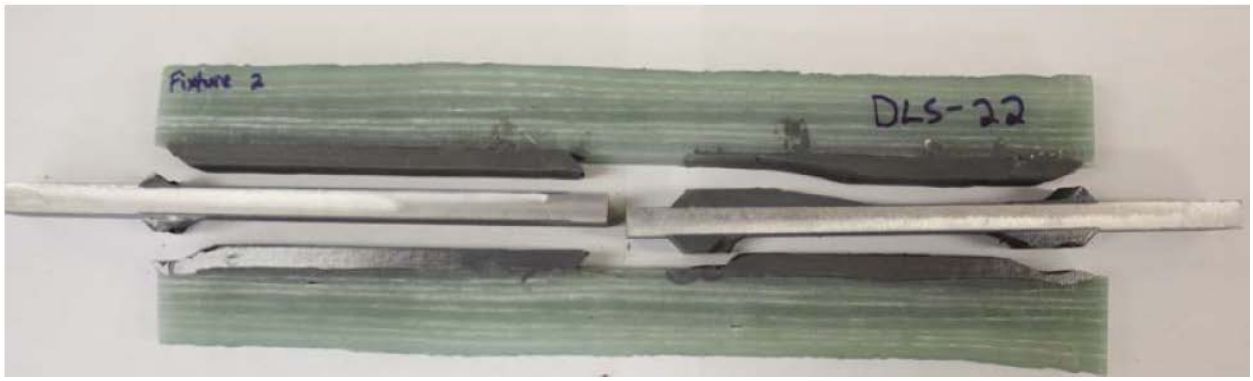

Figure 10 – Typical double lap shear static testing failure.

Mean and characteristic values of shear strength are presented in Table 7. Individual test results are presented as Appendix 7.2. The characteristic values are calculated as the mean of valid test results, minus a specified number (k_m) of standard deviations. Values of k_m were taken from C501 Table 4-3. A total of ten test results were rejected: five specimens were accidentally loaded at a rate 100 times slower than intended (DLS-5868-1,2,3,6,7); four specimens weren't given sufficient time to cure (DLS-5868-26,27,28,31), and; one specimen had an abnormal 'partial' failure (DLS-5868-11). In all rejected cases the tested response was relatively soft and weak.

The partial load effect factor for slamming pressure γ_F is taken as 1.5 and the partial resistance factor γ_M as 1.22, as discussed in 2.3.2. An additional partial resistance factor of 1.1 is assumed for seawater saturation, bringing the partial resistance factor up to 1.34. The load model and resistance model factors are taken to be unity for the ultimate limit of the DLS adhesive bond.

The relatively small number of valid test results, along with the level of variance expressed by the proportional standard deviation (pstd, see Table 7), resulted in inconsistent reductions in characteristic strength. While use of the characteristic values is important in design for risk mitigation, the mean shear strength may give a more accurate representation of the relative performance of the adhesive configurations. Considering the mean shear strength values, one sees that the shear strength tends to reduce with increased bondline thickness (0.25 in. Plexus contradicts this trend for reasons that are unclear).

All adhesive configurations tested exhibited sufficient strength to satisfy the characteristic ultimate stress of 2.35 MPa established in 2.4.2; using the characteristic design values, utilization ranges from 0.40 to 0.70.

Due to the long test times required for fatigue testing, it was necessary to down-select to two adhesive configurations. Mean shear strength values were used as the basis for down select, for reasons discussed above. Plexus MA560 and Araldite 2013 both exhibited high strength (11.8 and 11.7 MPa mean strength, respectively) at a relatively thick bondline (12.7 mm, or 0.50 in.) The only adhesive configuration with a higher mean strength was the 0.635 mm (0.25 in.) Araldite 2013; however, the higher tolerance requirements associated with the thinner bondline do not justify the moderate strength increase. Fatigue testing Araldite 2013 at both thicknesses was considered; while having comparative fatigue data at two bondline thicknesses would be informative, it was decided that having fatigue data for two different adhesive types provided greater value. Therefore 12.7mm (0.50 in.) Plexus MA560 and 12.7mm (0.50 in.) Araldite 2013 were down-selected for fatigue testing.

Table 7 – Characteristic shear strength of double lap shear joints.

Adhesive configuration	Units	Mean	std	pstd	N tests	k_m	Char. value	Utilization
Plexus 0.25 in.	MPa	10.9	0.34	0.031	4	3.2	9.79	0.48
Plexus 0.50 in.	MPa	11.8	0.35	0.030	5	2.9	10.8	0.44
Plexus 0.75 in.	MPa	11.5	0.86	0.075	5	2.9	8.98	0.53
Araldite 2013 0.25 in.	MPa	12.7	0.31	0.025	5	2.9	11.8	0.40
Araldite 2013 0.50 in.	MPa	11.7	1.55	0.132	4	3.2	6.76	0.70
Araldite 2015 0.25 in.	MPa	10.9	0.19	0.018	2	3.7	10.2	0.46
Araldite 2015 0.50 in.	MPa	10.8	0.44	0.041	2	3.7	9.16	0.52

3.2.2 Fatigue Limit

Two adhesive configurations were selected for fatigue testing; Plexus MA560-1 and Araldite 2013, both at 12.7mm (0.50 in.) bondline thickness. Testing was conducted following guidance from ASTM D3166 and is detailed in chapter 8 of the *Test Report* [4]. Fatigue analysis is based upon the fatigue test results (S-N data) and follows guidance from *DNVGL-RP-C203 Fatigue Design of Offshore Steel Structures* (C203) [8], and C501. The S-N curve formulation is given below in Figure 11 (C203 2.4.3).

The basic design S-N curve is given as

$$\log N = \log \bar{a} - m \log \Delta\sigma$$

N = predicted number of cycles to failure for stress range $\Delta\sigma$
$\Delta\sigma$ = stress range with unit MPa
m = negative inverse slope of S-N curve
$\log \bar{a}$ = intercept of log N-axis by S-N curve

Figure 11 – S-N curve formulation (DNVGL-RP-C203)

A total of 48 DLS specimens were fatigue tested, with maximum levels ranging from 31 to 90% of the mean ultimate load value. Specimens were cycled from 10 to 100% of the maximum load; thus in all cases, the stress range was 90% of the maximum stress. Note that the reference ultimate load values used to establish fatigue loadings were calculated when each adhesive configuration had only five DLS specimens tested; the final assessment of ultimate load changed somewhat with the 6th specimens tested, but nevertheless the load levels utilized for fatigue assessment were appropriate.

All fatigue testing was conducted at a 5 Hz cycling rate; a relatively low rate was used to ensure the specimens did not self-heat. The fatigue DLS specimens were identical to the ultimate load specimens; a nominal bond area of 7350 mm^2 (11.4 in^2) is assumed in calculating mean bondline stresses.

DLS specimens were cycled until failure, and typically the steel-to-adhesive bond was observed to be the primary failure. One DLS specimen (DLS-3166-13, Araldite 2013) was cycled 15.1e6 times with a maximum load of 20.5 kN (4.60 kips, or 25% of ultimate load) and was then removed from the load frame without failure. This specimen was later tested statically and failed at 10.5 MPa (0.81 standard deviations below the mean reported in Table 7). It is difficult to draw conclusions regarding an endurance limit from this single test result.

The results from all fatigue tests that cycled to failure are depicted below in Figure 12; there are 24 Plexus MA560 results, and 23 Araldite 2013. Results are plotted on log-log scales, as cycles-to-failure versus the

stress range at which they were cycled. Considering the fatigue test results, along with the ultimate stress obtained from static testing, a two-slope S-N curve was assumed.

A subset of stress ranges (mid- to high-cycle region) was selected for fitting the primary S-N curve; these data are indicated by blue circles in Figure 12. A least-squares fit was performed on these data, providing a mean S-N curve for the mid- to high-cycle region. Note that one Araldite result was rejected as an outlier (plotted as a yellow 'x'). A least-squares fit was performed on the remaining low-cycle data, with the result constrained to pass through the mean ultimate stress from static testing.

Similar to the characteristic design values discussed above, design S-N curves were also assessed. Following guidance provided in Appendix F.7 of C203, the mean S-N curve was shifted by a specified number (c) of standard deviations of test data $\log_{10}$ N. The standard deviation of the primary S-N curve data was used (mid- to high-cycle). The value of c was interpolated from C203 Table F-3, for a 95% confidence level where the standard deviation was not known *a priori*. Relevant parameters characterizing the mean and design S-N curves are presented in Table 8.

Fatigue life was calculated as a Miner's sum, assuming a Weibull shape factor of 1.0. A mean zero-upcrossing period of 6.68 s was calculated for the prototype deployment site, assuming a Pierson-Moskowitz spectral shape and a ratio of mean zero-upcrossing period(T_z) to energy period (T_e) of 0.827. The fatigue life calculations assume that the stress response period is characterized by the zero-upcrossing period.

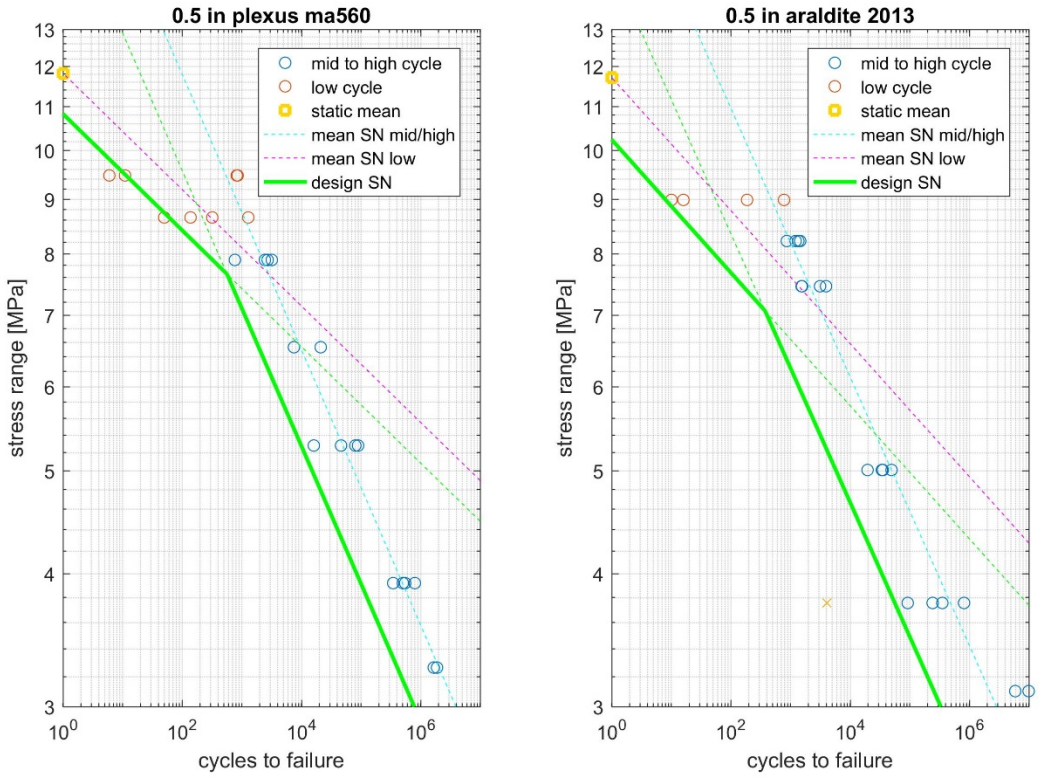

Figure 12 – Fatigue data and SN curves for 0.5 in. Plexus MA560 and Araldite 2013.

Table 8 – S-N curve parameters and fatigue life.

	Plexus MA560, 0.5 in.	Araldite 2013, 0.5 in.
Valid test results, total	24	22
Valid test results, mid- to high-cycle	16	18
Standard deviation of $\log_{10}$ N, mid- to high- cycle	0.231	0.316
Design offset factor, c	3.03	2.96
Mid- to high-cycle S-N curve, primary curve		
Negative inverse slope	7.73	7.92
Intercept of $\log_{10}$ N axis, mean curve	10.3	10.2
Intercept of $\log_{10}$ N axis, design curve	9.58	9.31
Low-cycle S-N curve		
Negative inverse slope	18.3	16.0
Intercept of $\log_{10}$ N axis, mean curve	19.6	17.1
Intercept of $\log_{10}$ N axis, design curve	18.9	16.2
Fatigue life		
Fatigue life [years]	1930	890

The maximum stress range is derived from the slamming load case (DLC 6, see 2.4.2), which is the maximum stress predicted from a 50-year return storm conditions. An assumption of a fully reversing stress for the maximum stress range is conservative, as a slamming event is certainly not symmetrical.

Table 8 above gives calculated fatigue life for the adhesive joint for maximum stress range of 4.70 MPa (fully reversing).

Based on the design S-N curves derived from DLS fatigue testing, the fatigue life of the adhesive joint under the most conservative assumption of fully reversing maximum stress is 1930 and 890 years for Plexus MA560 and Araldite 2013, respectively. Fatigue calculations are presented as Appendix 7.3.

Considering that the prototype WEC has a design life of 5 years, and that the eventual commercial WEC will have a design requirement of a 20-year life, this fatigue analysis supports the feasibility of the DLS adhesive joint design using either adhesive configuration tested.

4 HYBRID STRUCTURE IMPACT

This section estimates the impact of a hybrid FRP/steel structure on the prototype H2 WEC in terms of cost and weight.

Estimated costs are for fabrication only, and do not include engineering, coatings, delivery, installation, etc. Estimated mass assumes a density of 7800 kg/m^3 for steel; using measured ply density and thickness values from Table 3, the density for the optimized laminate is calculated as 1810 kg/m^3. Cost and weight estimates are for those sections of the hull components that are being considered for replacement with FRP (e.g., the portion of a pontoon that extends between the interior watertight bulkheads).

Cost and weight estimates for a pontoon are detailed below in Table 9. The prototype WEC steel pontoon, including ring frame internal stiffeners, is described in *WEC Design Documentation* [5] and depicted in *WEC Structural Arrangement* [6]. The steel pontoon cost estimate assumes a labor rate of 75 $/hour, a fabrication rate of 150 hours/long ton, and a material cost of 0.754 $/lb. The steel pontoon section has a mass of 8400 kg, and an estimated fabrication cost of $107k.

Table 9 – Pontoon cost and weight comparison for prototype H2 WEC.

	Units	Steel	FRP
Length	m	7.90	7.90
Diameter	m	3.82	3.82
Thickness	m	0.0111	0.0294
Stiffeners	m^3	0.0245	0
Density	kg/m^3	7800	1810
Mass	kg	8410	5040
Cost	k$	107	60.4

An FRP pontoon section with the optimized layup described in 2.4.1 has a mass of 5040 kg, representing a 40% mass reduction with respect to the steel alternative. The estimated fabrication cost for the FRP pontoon section is $57.2k (quote from Ershigs [9]). Supplier quotes for the two candidate adhesives indicate similar cost, with a pair of 50-gallon drums (one each of resin and hardener) costing $12.7k and $11.9k for Plexus MA560 [10] and Araldite 2013 [11], respectively. An estimated 27.1 gallons of adhesive is needed for the two DLS joints associated with each pontoon, bringing the cost estimate for an FRP pontoon section to $60.4k, and representing a 44% cost reduction with respect to the steel alternative (Araldite 2013 cost used for estimate).

There are several hull components with significant structural similarities to the pontoons (see Figure 13). The lower spars and knee braces are also cylindrical sections, which along with the pontoons form structural triangles. The upper spars are cylindrical sections extending upwards from the pontoons. Although not investigated explicitly within this project, it is reasonable to assume that a similar hybrid construction could readily be adapted for these components as well. The float, ballast tank, and nacelle are also cylindrical sections, but have significantly greater complexity in internal interfaces and are not considered candidates for obvious extension of this hybrid construction (i.e. simple cylindrical section with DLS interface with complex steel joint section).

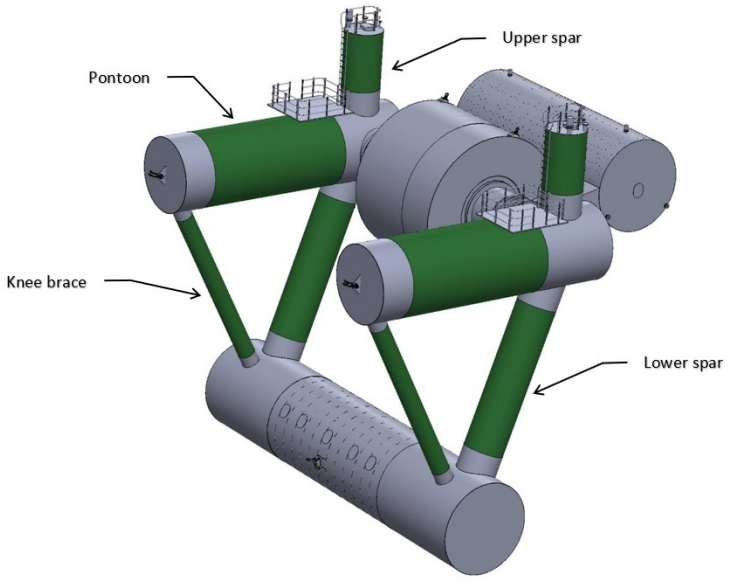

Figure 13 – Subcomponents identified for hybrid FRP / steel fabrication.

Cost and weight comparison between steel and FRP are detailed below in Table 10, for lower spar, upper spar, and knee brace sections. Rather than developing layup schedules for each of these sections, an assumption was made that required FRP thickness is proportional to the required steel thickness determined in prototype design. The estimated cost of the steel and FRP sections are assumed to be proportional to their mass.

Total mass and fabrication costs for steel and FRP, per WEC, are detailed in Table 11. Assuming hybrid steel / FRP pontoons, there is an estimated savings of 6.74 tonnes and $93.3k per WEC. Assuming hybrid fabrication of pontoons, upper and lower spars, and knee braces there is an estimated savings of 13.0 tonnes and $181k per WEC. Note that the impact on project metrics will be covered in the Final Technical Report.

Table 10 – Lower / upper spar and knee brace cost and weight comparison for prototype H2 WEC.

		Lower spar		Upper spar		Knee brace	
		Steel	**FRP**	**Steel**	**FRP**	**Steel**	**FRP**
Length	m	6.60	6.60	2.90	2.90	9.60	9.60
Diameter	m	1.98	1.98	1.98	1.98	0.900	0.900
Thickness	mm	0.00953	0.0252	0.00635	0.0168	0.0191	0.0505
Stiffeners	m^3	0.00575	0	0.00192	0	0	0
Density	kg/m^3	7800	1810	7800	1810	7800	1810
Mass	kg	3100	1870	909	548	4030	2470
Cost	k$	39.4	22.4	11.6	6.57	51.4	29.7

Table 11 – Cost and weight comparison for prototype H2 WEC with hybrid structure.

	Mass [tonne]		Cost [k$]	
	Steel	**FRP**	**Steel**	**FRP**
Pontoons only	16.8	10.1	214	121
Pontoons, upper and lower spars, knee braces	32.9	19.9	419	238

5 CONCLUSIONS

Extensive coupon testing was performed on potential constituent materials for a conceptual hybrid hull design (fiber-reinforced plastic pontoon and steel). Test results were analyzed following guidance from *DNVGL ST C501*, and characteristic material property values were calculated.

Finite element analysis was performed, utilizing the characteristic material properties, to optimize the conceptual laminate design and to assess the maximum bondline stress. Loading and boundary conditions were adapted from the steel prototype design. The slamming design load case dominated, and for the optimized laminate resulted in a Tsai Wu Failure Criteria of 0.88 and a maximum discretized bondline stress of 2.35 MPa. The resulting optimized laminate [1FW,7(1U,2FW),1U,1FW] utilizes fewer layers overall than the concept design [1FW,9(1U,2FW)].

Static and fatigue testing was performed on full-scale, sectioned, double lap shear (DLS) joint specimens. Three different adhesives were tested at bondline thicknesses ranging from 6.35 to 19.0 mm (0.250 to 0.750 in.). An adhesive capable of supporting a characteristic ultimate stress of 2.35 MPa, while allowing for larger bondline thicknesses, was desired.

Static DLS test specimens were loaded to failure; typically, the steel-to-adhesive bond observed to be the primary failure. Mean and characteristic ultimate strengths were calculated for the eight different adhesive configurations tested. Two adhesives (Plexus MA560 and Araldite 2013) exhibited high mean strength (11.8 and 11.7 MPa respectively) at 12.7 mm (0.500 in.) bondline thickness and were selected to advance to fatigue testing. Due to the variability and number of test results, the characteristic strengths were reduced to 10.8 and 6.76 MPa for Plexus MA560 and Araldite 2013, respectively. Both of these adhesives are adequate for the design ultimate limit; with all safety factors considered, the Plexus and Araldite DLS specimens were assessed at 0.44 and 0.70 utilization, respectively.

Fatigue DLS test specimens were cycled to failure at various stress ranges, enabling the development of fatigue response models (S-N curves). Again, the steel-to-adhesive bond was typically observed to be the primary failure. Mean and characteristic (design) S-N curves were developed. Fatigue life was calculated as a Miner's sum using a maximum stress range derived from the maximum stress predicted from 50-year return storm conditions. Fatigue life was calculated as 1930 and 890 years (for Plexus MA560 and Araldite 2013 respectively), with a conservative assumption of fully reversing stress from the slamming load case that is driving the design. Considering that the prototype WEC has a design life of 5 years, and that the eventual commercial WEC will have a design requirement of a 20-year life, this fatigue analysis supports the feasibility of the DLS adhesive joint design using either Plexus MA560 or Araldite 2013.

Note that the effect of seawater saturation on adhesive performance was not investigated within this project. C·Power intends to explore options for future testing of seawater saturated DLS test specimens.

Mass and cost savings for a prototype-scale H2 WEC with hybrid steel / FRP pontoons are estimated to be 6.74 tonnes and $90.8k. Extending the hybrid design to structurally analogous components (upper and lower spars, and knee braces) results in estimated mass and cost savings of 13.0 tonnes and $176k.

6 REFERENCES

[1] "Test Article Design Technical Memo," Glosten, 18024.01-200–01 Rev. A, Oct. 2018.

[2] "Composite Components," DNV GL, DNVGL-ST-C501, Aug. 2017.

[3] "WEC Pontoon Design Alternative Composites Coupon Panels," Glosten, 18024-100–20 Rev. B, Nov. 2018.

[4] "CPower Coupon and Double Lap Shear Specimen Test Report," National Renewable Energy Laboratory, Sep. 2019.

[5] "CPower WEC Design Documentation," Glosten, 18024-10-100 Rev. A, Jun. 2019.

[6] "CPower WEC Structural Arrangement," Glosten, 18024-100–01 Rev. B, Apr. 2019.

[7] M. Y. Tsai, D. W. Oplinger, and J. Morton, "Improved Theoretical Solutions for Adhesive Lap Joints," *Int J Solids Struct.*, vol. 35, no. 12, pp. 1163–1185, 1998.

[8] "Fatigue Design of Offshore Steel Structures," DNV GL, DNVGL-RP-C203, Apr. 2016.

[9] S. Spencer (Ershigs), email to P. Lenee-Bluhm, "Re: CPT WEC testing," 01-Oct-2019.

[10] T. Post (ITW), email to P. Lenee-Bluhm, "Re: Plexus MA 560 cost," 23-Aug-2019.

[11] A. Mansfield (Huntsman), email to P. Lenee-Bluhm, "Re: Columbia Power Technologies 08292019 (1)," 29-Aug-2019.

7 APPENDICES

7.1 Appendix: Tsai Wu Failure Criteria distributions

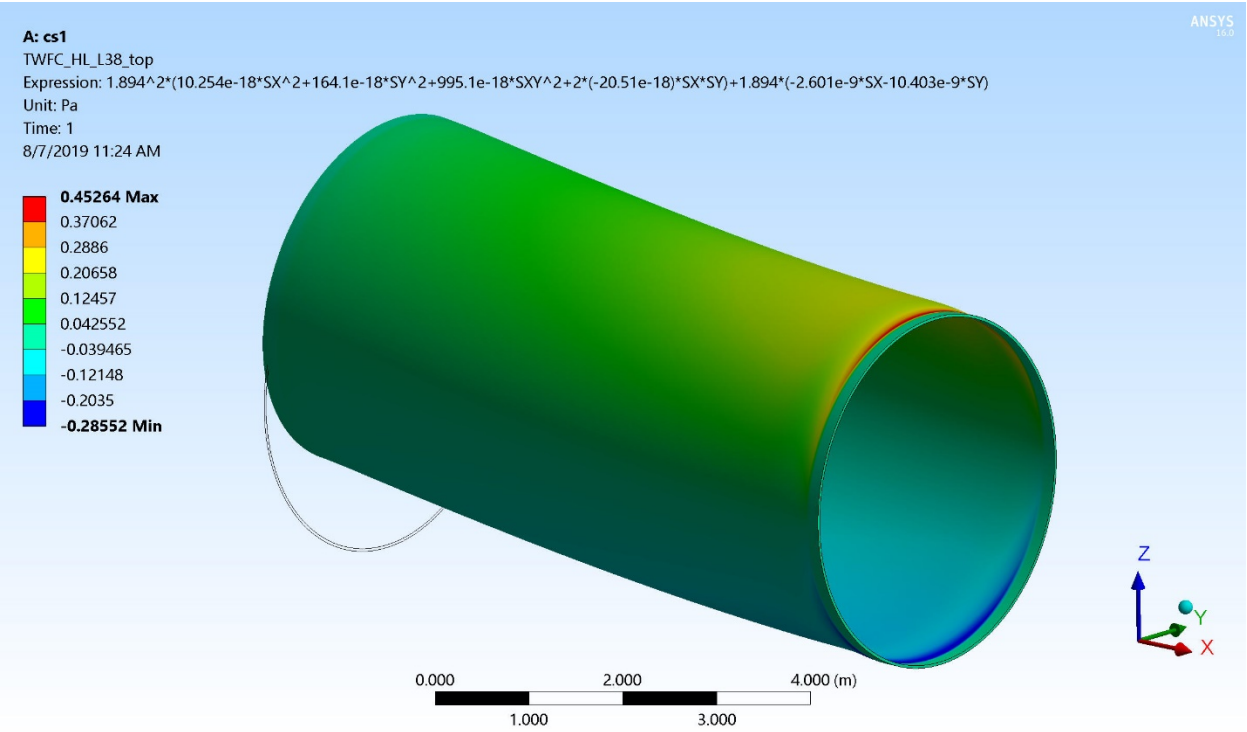

Figure 14 – Tsai Wu Failure Criteria for max. bending design load case (DLC 1).

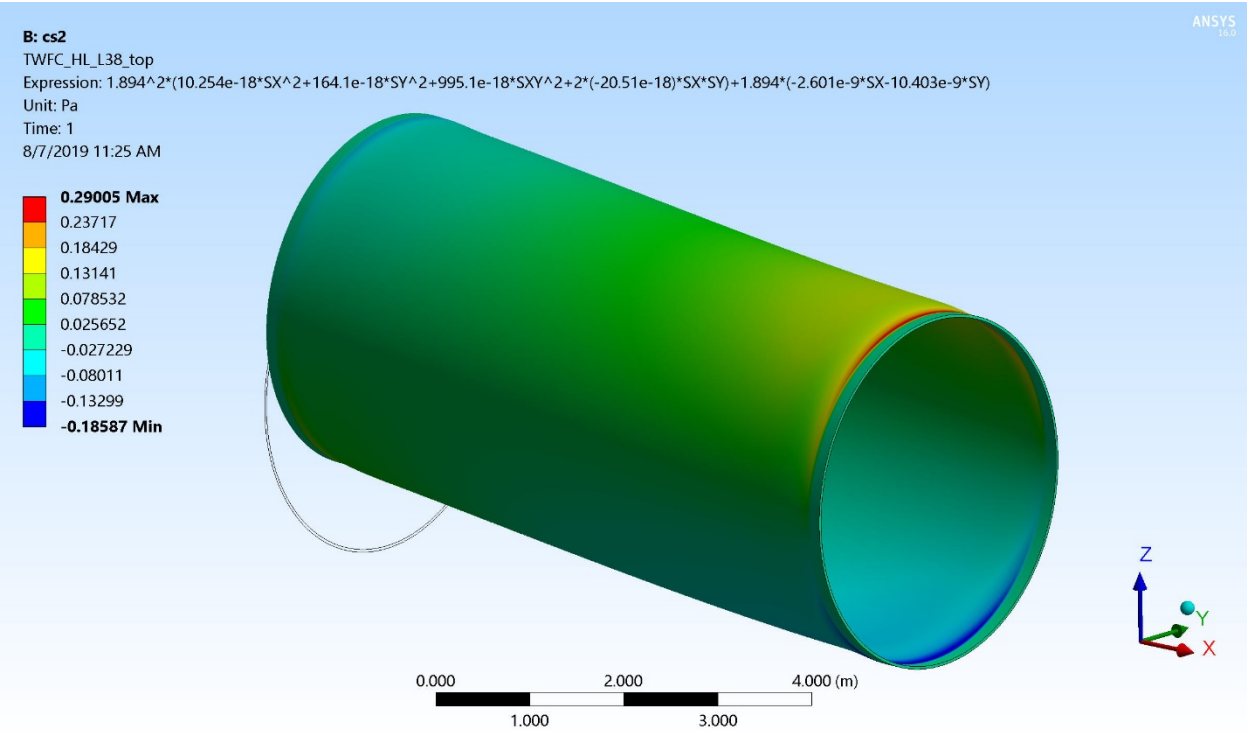

Figure 15 – Tsai Wu Failure Criteria for max. shear design load case (DLC 2).

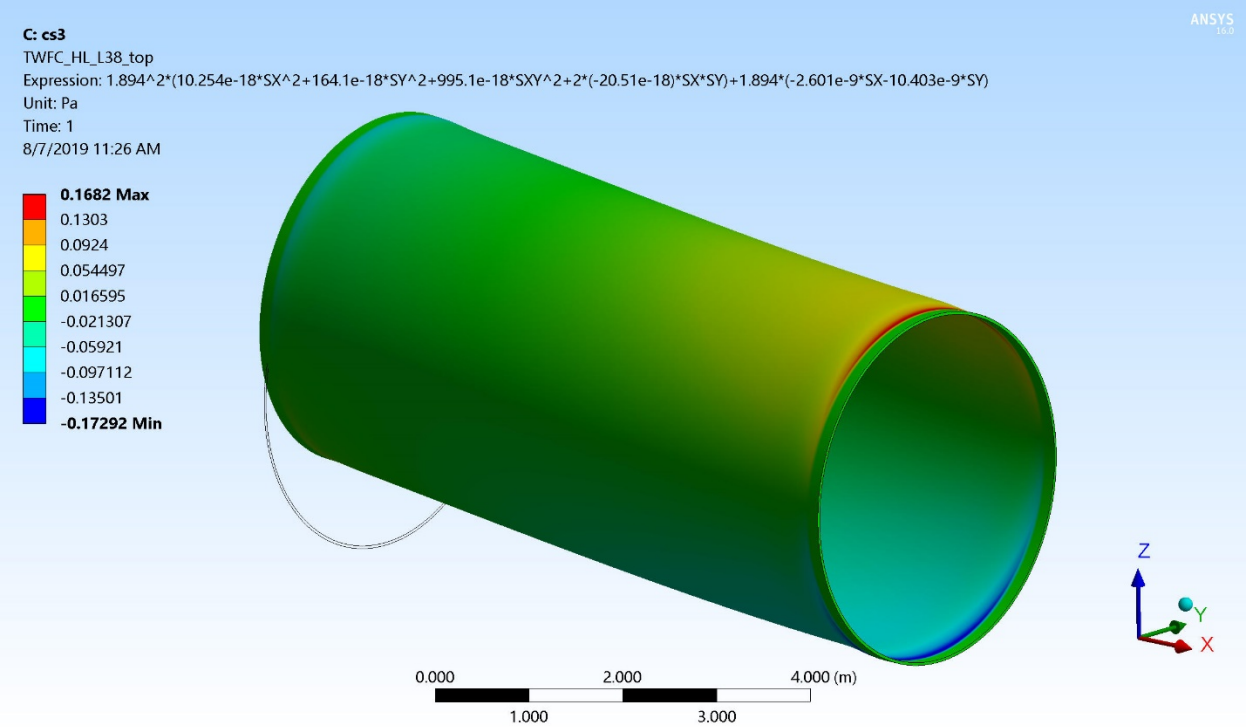

Figure 16 – Tsai Wu Failure Criteria for max. axial (tension) design load case (DLC 3).

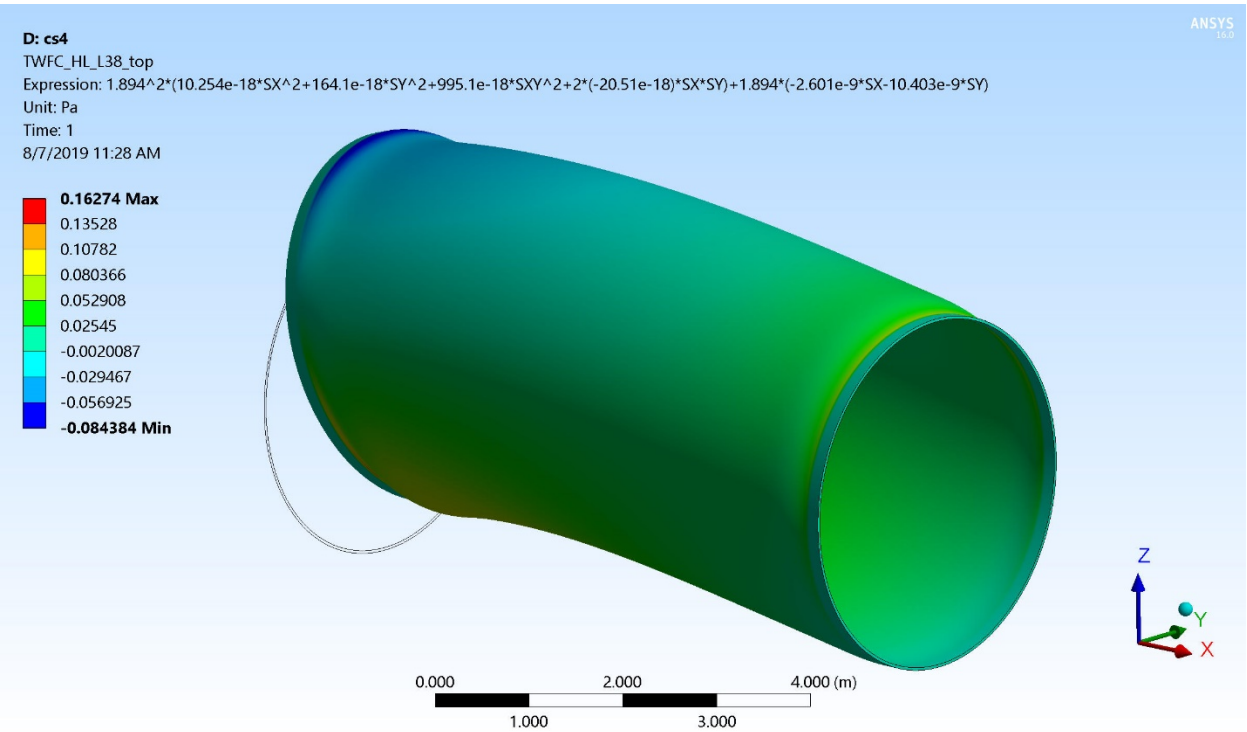

Figure 17 – Tsai Wu Failure Criteria for max. axial (compression) design load case (DLC 4).

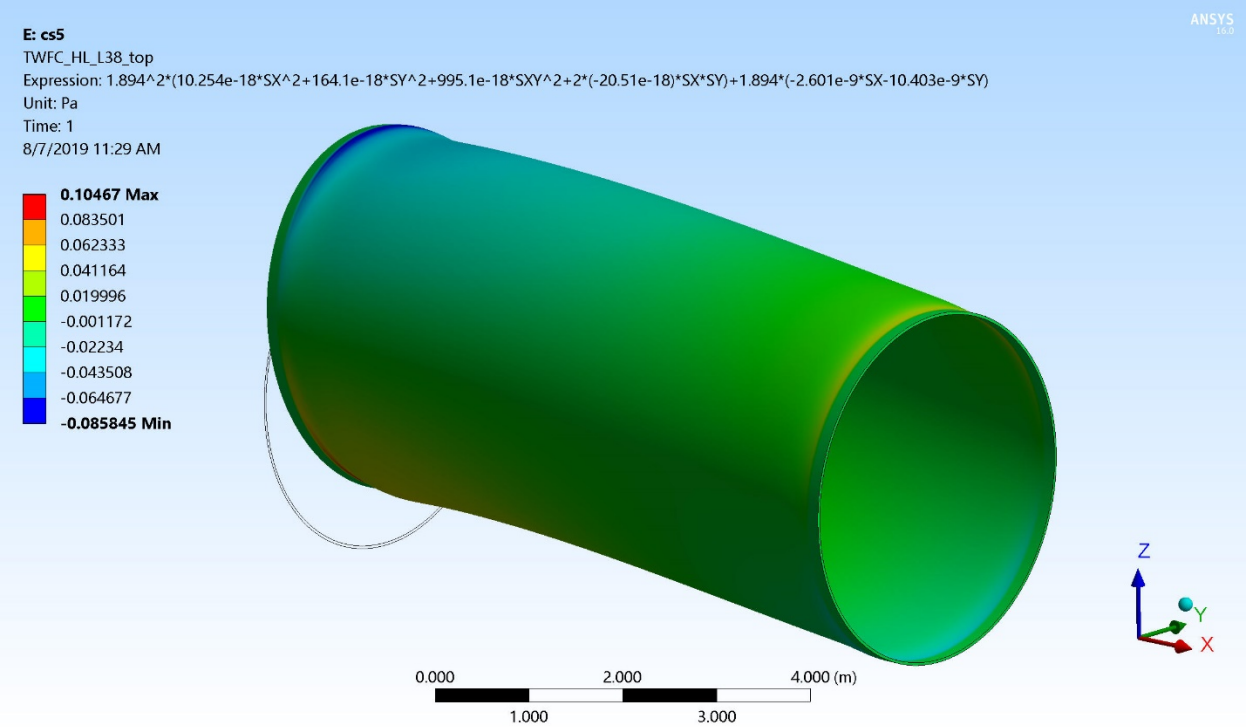

Figure 18 – Tsai Wu Failure Criteria for max. torsion design load case (DLC 5).

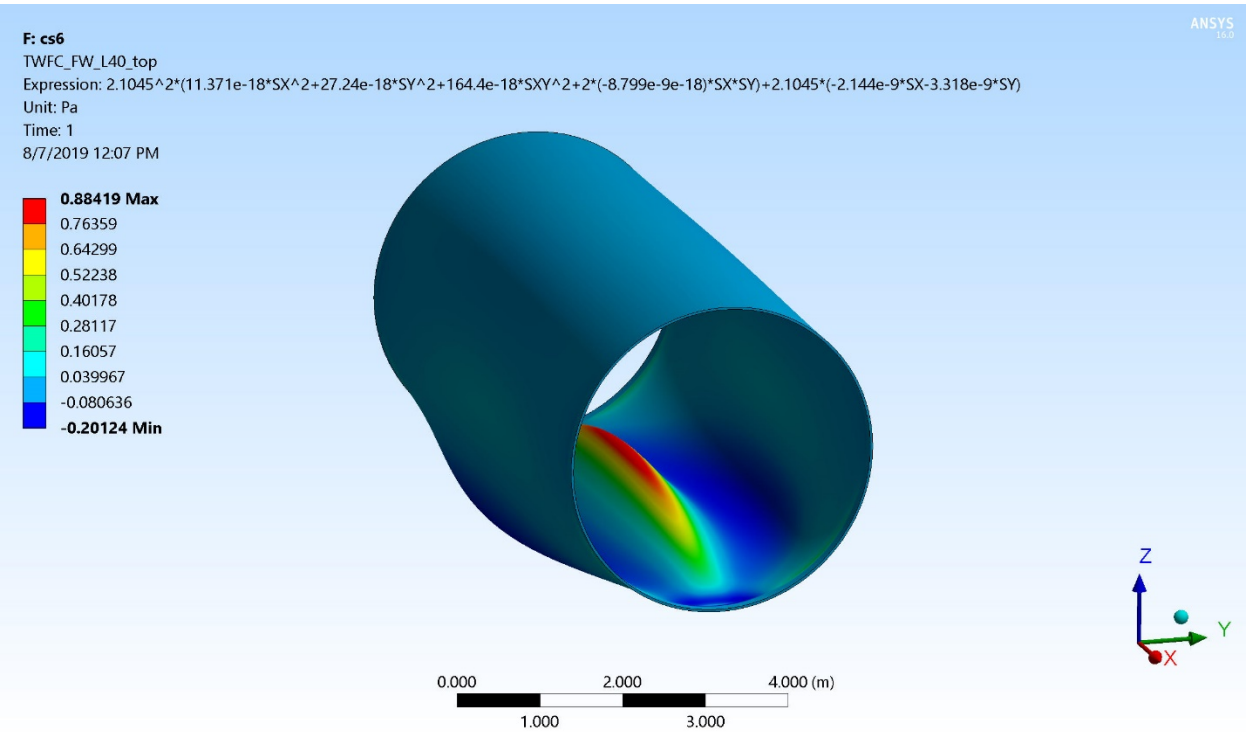

Figure 19 – Tsai Wu Failure Criteria for max. slamming design load case (DLC 6).

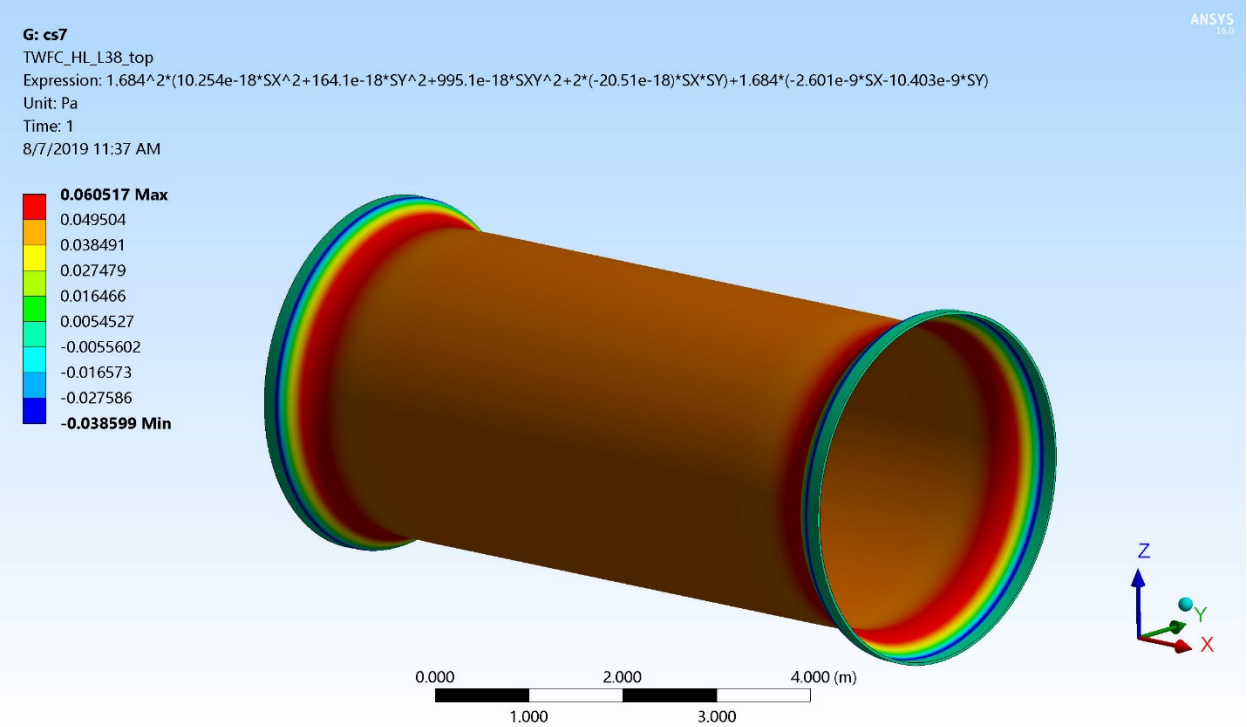

Figure 20 – Tsai Wu Failure Criteria for max. submersion (hydrostatic) design load case (DLC 7).

7.2 Appendix: DLS Static Assessment

Table 12 – DLS static test results.

Glosten Number	NREL Number	Adhesive	Bondline Thickness	Date Prepared	Date Tested	UTS load [lbs]	UTS load [kN]	Strength [MPa]	Stiffness [lb/in]	Stiffness [kN/mm]	QC	Testing / Failure Notes
D5868-01	DLS-31	Plexus	0.25	3/27/2019	3/29/2019	15,364	68.34	9.292	234,935	41.14	0	Appeared significanly more elastic failure compared to other specimens, perhaps too short cure time
D5868-02	DLS-32	Plexus	0.25	3/27/2019	4/2/2019	18,412	81.90	11.136	250,611	43.89	1	
D5868-03	DLS-33	Plexus	0.25	3/27/2019	4/2/2019	18,523	82.39	11.203	255,193	44.69	1	
D5868-04	DLS-34	Plexus	0.25	3/27/2019	4/2/2019	17,605	78.31	10.648	248,177	43.46	1	
D5868-05	DLS-35	Plexus	0.25	3/27/2019	4/2/2019	17,406	77.43	10.527	248,815	43.57	1	
					mean	17987	80.01	10.88	250,699	43.90	4	<-- N valid tests
					std	563	2.51	0.34	3,168	0.55	3.2	<-- km
					char val	16184	71.99	9.79	250,699	43.90		

Glosten Number	NREL Number	Adhesive	Bondline Thickness	Date Prepared	Date Tested	UTS load [lbs]	UTS load [kN]	Strength [MPa]	Stiffness [lb/in]	Stiffness [kN/mm]	QC	Testing / Failure Notes
D5868-06	DLS-11	Plexus	0.5	3/14/2019	3/27/2019	15,016	66.79	9.082	203,246	35.59	0	Incomplete failure
D5868-07	DLS-12	Plexus	0.5	3/14/2019	3/27/2019	19,383	86.22	11.723	211,745	37.08	1	
D5868-08	DLS-13	Plexus	0.5	3/14/2019	3/27/2019	19,248	85.62	11.641	212,511	37.22	1	
D5868-09	DLS-14	Plexus	0.5	3/14/2019	3/28/2019	18,952	84.30	11.462	210,261	36.82	1	
D5868-10	DLS-15	Plexus	0.5	3/14/2019	3/28/2019	19,674	87.51	11.899	214,511	37.57	1	
	D3166-39	Plexus	0.5	5/6/2019	5/20/2019	20,469	91.05	12.380	216,853	37.98	1	
					mean	19545	86.94	11.82	213,176	37.33	5	<-- N valid tests
					std	578	2.57	0.35	2,564	0.45	2.9	<-- km
					char val	17869	79.48	10.81	213,176	37.33		

Glosten Number	NREL Number	Adhesive	Bondline Thickness	Date Prepared	Date Tested	UTS load [lbs]	UTS load [kN]	Strength [MPa]	Stiffness [lb/in]	Stiffness [kN/mm]	QC	Testing / Failure Notes
D5868-11	DLS-16	Plexus	0.75	3/21/2019	3/27/2019	19,285	85.78	11.664	187,867	32.90	1	
D5868-12	DLS-17	Plexus	0.75	3/21/2019	3/27/2019	18,193	80.93	11.003	182,381	31.94	1	
D5868-13	DLS-18	Plexus	0.75	3/21/2019	3/27/2019	16,898	75.17	10.220	180,824	31.67	1	
D5868-14	DLS-19	Plexus	0.75	3/21/2019	3/28/2019	19,989	88.92	12.089	183,635	32.16	1	
D5868-15	DLS-20	Plexus	0.75	3/21/2019	3/28/2019	20,379	90.65	12.325	189,843	33.25	1	
					mean	18949	84.29	11.46	184,910	32.38	5	<-- N valid tests
					std	1416	6.30	0.86	3,801	0.67	2.9	<-- km
					char val	14843	66.03	8.98	184,910	32.38		

Glosten Number	NREL Number	Adhesive	Bondline Thickness	Date Prepared	Date Tested	UTS load [lbs]	UTS load [kN]	Strength [MPa]	Stiffness [lb/in]	Stiffness [kN/mm]	QC	Testing / Failure Notes
D5868-16	DLS-21	Huntsman 2013	0.25	3/22/2019	3/25/2019	21,364	95.03	12.921	281,714	49.34	1	Load frame paused at 20,367 for 5-10 seconds. Load removed, then test ran again until failure.
D5868-17	DLS-22	Huntsman 2013	0.25	3/22/2019	3/25/2019	20,517	91.26	12.409	294,121	51.51	1	
D5868-18	DLS-23	Huntsman 2013	0.25	3/22/2019	3/25/2019	21,139	94.03	12.785	285,375	49.98	1	
D5868-19	DLS-24	Huntsman 2013	0.25	3/25/2019	3/27/2019	21,717	96.60	13.135	294,670	51.60	1	Load frame maxed out at 21+ kip and stayed there for a few seconds before coupon broke. Ultimate load likely higher than failure load due to this reason. Picture of load/displacement available in DLS-24 folder.
D5868-20	DLS-25	Huntsman 2013	0.25	3/25/2019	3/27/2019	20,560	91.46	12.435	282,116	49.41	1	
					mean	21059	93.68	12.74	287,599	50.37	5	<-- N valid tests
					std	518	2.31	0.31	6,367	1.12	2.9	<-- km
					char val	19556	86.99	11.83	287,599	50.37		

Glosten Number	NREL Number	Adhesive	Bondline Thickness	Date Prepared	Date Tested	UTS load [lbs]	UTS load [kN]	Strength [MPa]	Stiffness [lb/in]	Stiffness [kN/mm]	QC	Testing / Failure Notes
D5868-21	DLS-06	Huntsman 2013	0.5	3/11/2019	3/19/2019	17,187	76.45	10.395	235,439	41.23	0	Low displacement rate (0.005 in/min)
D5868-22	DLS-07	Huntsman 2013	0.5	3/11/2019	3/20/2019	18,807	83.66	11.375	254,472	44.56	0	Low displacement rate (0.005 in/min)
D5868-23	DLS-08	Huntsman 2013	0.5	3/11/2019	3/20/2019	19,368	86.15	11.714	272,978	47.81	1	
D5868-24	DLS-09	Huntsman 2013	0.5	3/11/2019	3/21/2019	16,280	72.42	9.846	265,859	46.56	1	
D5868-25	DLS-10	Huntsman 2013	0.5	3/8/2019	3/21/2019	19,265	85.69	11.652	268,075	46.95	1	
	D3166-5	Huntsman 2013	0.5	4/11/2019	5/22/2019	22,547	100.29	13.636	259,043	45.37	1	
					mean	19365	86.14	11.71	266,489	46.67	4	<-- N valid tests
					std	2559	11.39	1.55	5,787	1.01	3.2	<-- km
					char val	11175	49.71	6.76	266,489	46.67		

Glosten Number	NREL Number	Adhesive	Bondline Thickness	Date Prepared	Date Tested	UTS load [lbs]	UTS load [kN]	Strength [MPa]	Stiffness [lb/in]	Stiffness [kN/mm]	QC	Testing / Failure Notes
D5868-26	DLS-26	Huntsman 2015	0.25	3/26/2019	3/27/2019	15,414	68.56	9.322	232,618	40.74	0	Only 1 day cure time
D5868-27	DLS-27	Huntsman 2015	0.25	3/26/2019	3/27/2019	16,706	74.31	10.104	235,560	41.25	0	Only 1 day cure time
D5868-28	DLS-28	Huntsman 2015	0.25	3/26/2019	3/27/2019	16,114	71.68	9.746	233,696	40.93	0	Only 1 day cure time
D5868-29	DLS-29	Huntsman 2015	0.25	3/26/2019	3/28/2019	17,785	79.11	10.756	276,940	48.50	1	
D5868-30	DLS-30	Huntsman 2015	0.25	3/26/2019	3/28/2019	18,234	81.11	11.028	280,599	49.14	1	
					mean	18010	80.11	10.89	278,770	48.82	2	<-- N valid tests
					std	317	1.41	0.19	2,587	0.45	3.7	<-- km
					char val	16835	74.88	10.18	278,770	48.82		

Glosten Number	NREL Number	Adhesive	Bondline Thickness	Date Prepared	Date Tested	UTS load [lbs]	UTS load [kN]	Strength [MPa]	Stiffness [lb/in]	Stiffness [kN/mm]	QC	Testing / Failure Notes
D5868-31	DLS-01	Huntsman 2015	0.5	3/13/2029	3/19/2019	12,834	57.09	7.762	240,522	42.12	0	Low displacement rate (0.005 in/min)
D5868-32	DLS-02	Huntsman 2015	0.5	3/13/2029	3/19/2019	11,692	52.01	7.071	237,014	41.51	0	Low displacement rate (0.005 in/min)
D5868-33	DLS-03	Huntsman 2015	0.5	3/13/2029	3/20/2019	15,543	69.14	9.400	251,091	43.97	0	Low displacement rate (0.005 in/min)
D5868-34	DLS-04	Huntsman 2015	0.5	3/13/2029	3/21/2019	17,324	77.06	10.478	258,408	45.25	1	
D5868-35	DLS-05	Huntsman 2015	0.5	3/13/2029	3/21/2019	18,351	81.63	11.099	255,481	44.74	1	
					mean	17838	79.35	10.79	256,945	45.00	2	<-- N valid tests
					std	726	3.23	0.44	2,070	0.36	3.7	<-- km
					char val	15151	67.39	9.16	256,945	45.00		

7.3 Appendix: DLS Fatigue Assessment

Table 13 – DLS fatigue life calculations.

assume weibull distribution with factor of 1

Sdes	2.35	MPa	fatigue design stress... no sfs applied
	2		stress reversal factor
Sc	4.7	MPa	max stress range, assuming partially reversing cycles (conservative)
N	2.36E+08		load cycles in 50 yr span
k	1		weibull parameter

The basic design S-N curve is given as

$$\log N = \log \bar{a} - m \log \Delta\sigma \qquad (2.4.1)$$

N = predicted number of cycles to failure for stress range $\Delta\sigma$
$\Delta\sigma$ = stress range with unit MPa
m = negative inverse slope of S-N curve
$log\,\bar{a}$ = intercept of log N-axis by S-N curve

plexus ma560 (design fatigue curves)

	high cycle	low cycle	
log a	9.581	18.91	offset
m	7.725	18.28	slope
trans	7.65176	MPa	stress range transitioning between slopes
fat life	1927.24	yrs	
desgn life	20	yrs	
DFF	96		design fatigue factor

i	nc	ni	stress range lower	stress range upper	stress range mean	log(Ni)	Ni	ni/Ni
1	1	1	4.700	4.700	4.700	4.389	2.45E+04	0.0000
2	2	1	4.562	4.700	4.631	4.439	2.75E+04	0.0000
3	3	1	4.424	4.562	4.493	4.540	3.47E+04	0.0000
4	5	2	4.285	4.424	4.354	4.645	4.42E+04	0.0000
5	10	5	4.147	4.285	4.216	4.753	5.67E+04	0.0001
6	17	7	4.009	4.147	4.078	4.865	7.33E+04	0.0001
7	30	13	3.871	4.009	3.940	4.981	9.57E+04	0.0001
8	53	23	3.732	3.871	3.801	5.101	1.26E+05	0.0002
9	93	40	3.594	3.732	3.663	5.225	1.68E+05	0.0002
10	165	72	3.456	3.594	3.525	5.354	2.26E+05	0.0003
11	290	125	3.318	3.456	3.387	5.488	3.08E+05	0.0004
12	512	222	3.179	3.318	3.249	5.628	4.25E+05	0.0005
13	902	390	3.041	3.179	3.110	5.774	5.94E+05	0.0007
14	1,590	688	2.903	3.041	2.972	5.926	8.44E+05	0.0008
15	2,804	1,214	2.765	2.903	2.834	6.086	1.22E+06	0.0010
16	4,943	2,139	2.626	2.765	2.696	6.254	1.79E+06	0.0012
17	8,716	3,773	2.488	2.626	2.557	6.431	2.70E+06	0.0014
18	15,366	6,650	2.350	2.488	2.419	6.617	4.14E+06	0.0016
19	27,091	11,725	2.212	2.350	2.281	6.814	6.52E+06	0.0018
20	47,764	20,673	2.074	2.212	2.143	7.024	1.06E+07	0.0020
21	84,210	36,446	1.935	2.074	2.004	7.248	1.77E+07	0.0021
22	1.48E+05	6.43E+04	1.797	1.935	1.866	7.488	3.07E+07	0.0021
23	2.62E+05	1.13E+05	1.659	1.797	1.728	7.746	5.57E+07	0.0020
24	4.61E+05	2.00E+05	1.521	1.659	1.590	8.026	1.06E+08	0.0019
25	8.14E+05	3.52E+05	1.382	1.521	1.451	8.331	2.14E+08	0.0016
26	1.43E+06	6.21E+05	1.244	1.382	1.313	8.667	4.64E+08	0.0013
27	2.53E+06	1.09E+06	1.106	1.244	1.175	9.040	1.10E+09	0.0010
28	4.46E+06	1.93E+06	0.968	1.106	1.037	9.460	2.88E+09	0.0007
29	7.86E+06	3.40E+06	0.829	0.968	0.899	9.940	8.71E+09	0.0004
30	1.39E+07	6.00E+06	0.691	0.829	0.760	10.500	3.16E+10	0.0002
31	2.44E+07	1.06E+07	0.553	0.691	0.622	11.173	1.49E+11	0.0001
32	4.31E+07	1.86E+07	0.415	0.553	0.484	12.017	1.04E+12	0.0000
33	7.60E+07	3.29E+07	0.276	0.415	0.346	13.145	1.40E+13	0.0000
34	1.34E+08	5.80E+07	0.138	0.276	0.207	14.859	7.23E+14	0.0000
35	2.36E+08	1.02E+08	(0.000)	0.138	0.069	18.545	3.51E+18	0.0000
						cumulative damage		0.03
						cycles to limit		9.10E+09
						actual fatigue life		1927.24 years

araldite 2013 (design fatigue curves)

	sig<=trans	sig>trans	
log a	9.306	16.16	offset
m	7.922	15.99	slope
trans	7.05946	MPa	stress range transitioning between slopes
fat life	889.67	yrs	
desgn life	20	yrs	
DFF	44		design fatigue factor

i	nc	ni	stress range lower	stress range upper	stress range mean	log(Ni)	Ni	ni/Ni
1	1	1	4.700	4.700	4.700	3.981	9.58E+03	0.00
2	2	1	4.562	4.700	4.631	4.032	1.08E+04	0.00
3	3	1	4.424	4.562	4.493	4.136	1.37E+04	0.00
4	5	2	4.285	4.424	4.354	4.244	1.75E+04	0.00
5	10	5	4.147	4.285	4.216	4.355	2.26E+04	0.00
6	17	7	4.009	4.147	4.078	4.470	2.95E+04	0.00
7	30	13	3.871	4.009	3.940	4.588	3.88E+04	0.00
8	53	23	3.732	3.871	3.801	4.711	5.14E+04	0.00
9	93	40	3.594	3.732	3.663	4.839	6.90E+04	0.00
10	165	72	3.456	3.594	3.525	4.971	9.35E+04	0.00
11	290	125	3.318	3.456	3.387	5.109	1.28E+05	0.00
12	512	222	3.179	3.318	3.249	5.252	1.79E+05	0.00
13	902	390	3.041	3.179	3.110	5.402	2.52E+05	0.00
14	1,590	688	2.903	3.041	2.972	5.558	3.61E+05	0.00
15	2,804	1,214	2.765	2.903	2.834	5.722	5.27E+05	0.00
16	4,943	2,139	2.626	2.765	2.696	5.894	7.83E+05	0.00
17	8,716	3,773	2.488	2.626	2.557	6.075	1.19E+06	0.00
18	15,366	6,650	2.350	2.488	2.419	6.266	1.85E+06	0.00
19	27,091	11,725	2.212	2.350	2.281	6.469	2.94E+06	0.00
20	47,764	20,673	2.074	2.212	2.143	6.684	4.83E+06	0.00
21	84,210	36,446	1.935	2.074	2.004	6.913	8.19E+06	0.00
22	1.48E+05	6.43E+04	1.797	1.935	1.866	7.159	1.44E+07	0.00
23	2.62E+05	1.13E+05	1.659	1.797	1.728	7.424	2.65E+07	0.00
24	4.61E+05	2.00E+05	1.521	1.659	1.590	7.711	5.14E+07	0.00
25	8.14E+05	3.52E+05	1.382	1.521	1.451	8.024	1.06E+08	0.00
26	1.43E+06	6.21E+05	1.244	1.382	1.313	8.368	2.33E+08	0.00
27	2.53E+06	1.09E+06	1.106	1.244	1.175	8.751	5.63E+08	0.00
28	4.46E+06	1.93E+06	0.968	1.106	1.037	9.181	1.52E+09	0.00
29	7.86E+06	3.40E+06	0.829	0.968	0.899	9.674	4.72E+09	0.00
30	1.39E+07	6.00E+06	0.691	0.829	0.760	10.248	1.77E+10	0.00
31	2.44E+07	1.06E+07	0.553	0.691	0.622	10.939	8.69E+10	0.00
32	4.31E+07	1.86E+07	0.415	0.553	0.484	11.804	6.36E+11	0.00
33	7.60E+07	3.29E+07	0.276	0.415	0.346	12.961	9.14E+12	0.00
34	1.34E+08	5.80E+07	0.138	0.276	0.207	14.719	5.23E+14	0.00
35	2.36E+08	1.02E+08	(0.000)	0.138	0.069	18.498	3.15E+18	0.00
						cumulative damage		0.06
						cycles to limit		4.20E+09
						actual fatigue life		889.67